J Nanostruct 9(3): 579-586, Summer 2019

RESEARCH PAPER

Magnetic and Microwave Absorption Properties of Barium Hexaferrite Doped with La^{3+} and Gd^{3+}

Fatemeh Abdollahi [1], Mohammad Yousefi [2,], Malak Hekmati [3], Ana Khajehnezhad [1], Seyyed Salman Seyyed Afghahi [4]*

[1] *Department of Chemistry, Science and Research Branch, Islamic Azad University, Tehran, Iran*

[2] *Department of Chemistry, Yadegar-e- Imam Khomeini(RAH) Shahr-e- Rey Branch, Islamic Azad University, Tehran, Iran*

[3] *Department of Organic Chemistry, Faculty of Pharmaceutical chemistry, Tehran Medical Sciences, Islamic Azad University, Tehran, Iran*

[4] *Department of Engineering, Imam Hossein University, Tehran, Iran*

ARTICLE INFO

Article History:
Received 14 December 2018
Accepted 23 March 2019
Published 01 July 2019

Keywords:
Auto-Combustion
Electromagnetic Absorbing Materials
Hexaferrite
Reflection Loss
Sol-Gel

ABSTRACT

In this paper, $BaLa_xGd_xFe_{12-2x}O_{19}$ (x=0.2, 0.4, 0.6 and 0.8) were synthesized via sol-gel auto-combustion method. Fourier transform infrared spectroscopy (FTIR) of samples was represented that the bands at 400 and 500 cm^{-1} were related to the formation of hexaferrite phase. The (x-ray diffraction) XRD patterns were matched exactly with the structure of barium hexaferrite. (Field emission scanning electron microscopy) FESEM were represented the hexagonal shapes of all products. Magnetic analysis of barium hexaferrite were investigated by (vibrating sample magnetometer) VSM. The saturation magnetization of all samples decreased by increasing dopant's substitution due to the different occupation sites of dopants instead of Fe^{3+} (64 to 36.56 emu/g) in the hexaferrite structure. The coercivity increased because of its reverse relation with saturation magnetization (5010 to 5500 Oe). Microwave absorption properties of samples was investigated by (vector network analyzer) VNA. The maximum value of reflection loss was -7.8 db at 10.4 GHz frequency in 3mm thickness for x=0.4 sample.

How to cite this article
Abdollahi F, Yousefi M, Hekmati M, Khajehnezhad A, Seyyed Afghahi SS. Magnetic and Microwave Absorption Properties of Barium Hexaferrite Doped with La^{3+} and Gd^{3+}. J Nanostruct, 2019; 9(3): 579-586. DOI: 10.22052/JNS.2019.03.019

INTRODUCTION

Electromagnetic absorbing materials (EAM) were utilized to retain unwanted microwaves. Consequently, EMA has been developed in recent years for information security and to protect human in risky environments. EMA was classified into the resonant absorbers (ferrites) and the dielectric absorbers (foams). Due to the high thickness of dielectric absorbers, resonant absorbers were used as the practical electromagnetic absorbing materials.

One of the most promising and practical EMA are M-type hexagonal ferrites. Ferromagnetic barium hexaferrites were applied in different applications such as permanent magnets, data storage recording, electrical and microwave absorbing materials. M-type hexagonal ferrites were made from one R and one S block. The S block was composed of two spinel units ($MeFe_2O_4$) and the R block was made of three oxygen layers. In the middle of each layer, one of the oxygen atoms were substituted by barium atom. The unit formula of hexaferrites is SRS^*R^* in which * is the rotation of the block around *c* axis (1).

With their uniaxial anisotropy along *c* axis, the resonance frequency of barium hexaferrites is about 46 GHz. Fe^{3+} ions have occupied five various positions: octahedral sites (12k, 2a, and $4f_2$), tetrahedral site ($4f_1$) and trigonal bipyramidal site (2b) (2-6). For modifying the natural resonance frequency, magnetic and structure of barium hexaferrites, Fe^{3+} were substituted by divalent, trivalent and tetravalent ions

* *Corresponding Author Email: myousefi50@hotmail.com*

such as Co^{2+}–Ti^{4+}, Mg^{2+}–Ti^{4+}, Ni^{2+}–Ti^{4+}, Cr^{3+} ,and Ga^{3+} (7). The results were shown that magnetic properties of doped samples were changed significantly. Rare earth doping such as La^{3+} (8), Pr^{3+} (9), Nd^{3+} (10), Sm^{3+}(11), has been investigated widely because of the comparable ionic radius differences of Fe^{3+} and rare earth.

Many synthesis methods such as hydrothermal (12), co-perception (13) and sol-gel (14) were used for fabricating hexaferrites (15). Amongst them, sol-gel auto-combustion method was easily fabricated, convenient and cost-effective. Because barium hexaferrite doped with La^{3+} and Gd^{3+} were investigated rarely, for comparing and improving the absorption properties of samples, $BaLa_xGd_xFe_{12-2x}O_{19}$ (x=0.2, 0.4, 0.6 and 0.8) in consistent with pure hexaferrite were synthesized by easy and affordable sol-gel auto-combustion methods to obtain a series of novel samples with light weight and high electromagnetic absorbance percentage. $BaLa_xGd_xFe_{12-2x}O_{19}$ (x=0.2, 0.4, 0.6 and 0.8) were synthesized via sol-gel auto-combustion method and the magnetic and structural properties of all samples were investigated.

MATERIALS AND METHODS

$Ba(NO_3)_2$, $Fe(NO_3)_3$, $La(NO_3)_2$, $Gd(NO_3)_2$ and citric acid (all were purchased from Merck Company) was used for synthesis without any purification. Metal oxide salts and citric acid was dissolved in deionized water and then the solution was heated up to 80°C. Ammonium solution was added to adjust pH to 7. The solution was heated up to 110°C. After two hours elapsed, the gel ignited, and a brown powder was gained. The products was calcined at 900°C for 4 hours.

Sample preparation for VNA analysis

The samples were homogeneously dispersed in molten paraffin with the mass ratio of 70:30. The mixture were molded in the rectangular template with 22.86×10.16×3mm diameter.

Characterization

By using a Bruker-Tensor 27, the FTIR spectrum was obtained. The XRD patterns was revealed by utilizing Xpert diffractometer using CuK_α line radiation at 2ϑ scanning 20-80 with the step size of 0.02°. The FESEM micrographs was drawn by SIGMA VP-500, ZEISS model microscope. By utilizing VSM ZVK, R&S, the magnetic properties and hysteresis loops of samples were gained.

RESULTS AND DISCUSSIONS

FTIR spectrums

FTIR spectrums of samples were presented in Fig. 1. Two main bands at about 400 and 500 cm^{-1} are related to the vibrational modes of Fe-O in octahedral and tetrahedral structures. The

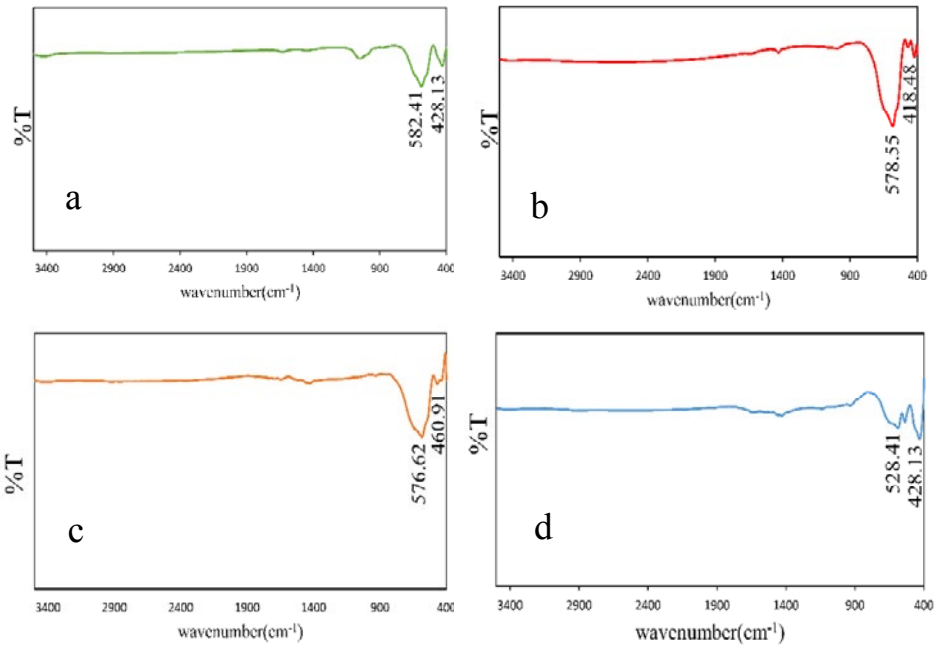

Fig. 1. FTIR $BaLa_xGd_xFe_{12-2x}O_{19}$ a) x=0.2, b) 0.4, c) 0.6 and d) 0.8

formation of hexaferrite were confirmed by these two main bands (16). By increasing the dopants, octahedral bands were shifted to the lower wavenumbers (582.41 to 528.41 cm^{-1}) due to the heavier mass of dopants.

XRD analysis

The XRD patterns of all samples were shown in Fig. 2. XRD patterns have confirmed the formation of hexaferrite structure in all samples which matched with JCPDS NO 43-0002 (17). The cell volume and the lattice parameters were calculated from the equations (1) and (2):

$$\frac{1}{d^2}=\frac{4}{3}\left(\frac{h^2+hk+k^2}{a^2}\right)+\frac{l^2}{c^2} \quad (1)$$

$$V=\frac{\sqrt{3}}{2}a^2c \quad (2)$$

Where d is the crystal plane distance, *a, and c* are lattice parameters, *h*, *k* and *l* are Miller indices and *V* is the cell volume (18). Due to the larger radius of La^{3+} (1.22Å) and Gd^{3+} (1.07Å) in comparison to the Fe^{3+} (0.63Å), the crystallite data (*a, c*) of $BaLa_xGd_xFe_{12-2x}O_{19}$ (x=0.2, 0.4, 0.6 and 0.8) were enhanced by increasing dopants substitution. As a result, the cell volume of samples were increased by substitution of dopants (643.60 to 664.63 A^3) (19). The ratio of *c/a* in all samples was about 3.95, which is matched completely with the value of M-type hexaferrites.

According to Scherer's equation which *k* (0.89) is constant, λ (1.540Å) is the wavelength of the X-ray radiation, ϑ refer to diffraction angle and β is the FWHM)(20) , the crystallite size of nanoparticles crystal size were 68.90, 82.31, 98.46, 117.73, 119.25 nm for 0.0, 0.2, 0.4, 0.6 and 0.8 dopants which confirm the nanometric scale of synthesized powders. By ascending the number of dopants,

Table 1. Lattice parameters of $BaLa_xGd_xFe_{12-2x}O_{19}$ (x=0.2, 0.4, 0.6 and 0.8)

sample	*a (Å)*	*c (Å)*	*c/a*	Crystallite size (nm)	*V(A^3)*
X=0.0	5.86	23.19	3.95	68.90	643.60
X=0.2	5.89	23.21	3.94	82.31	644.16
X=0.4	5.91	23.25	3.93	98.46	649.66
X=0.6	5.92	23.28	3.93	117.73	652.70
X=0.8	5.97	23.31	3.90	119.25	664.63

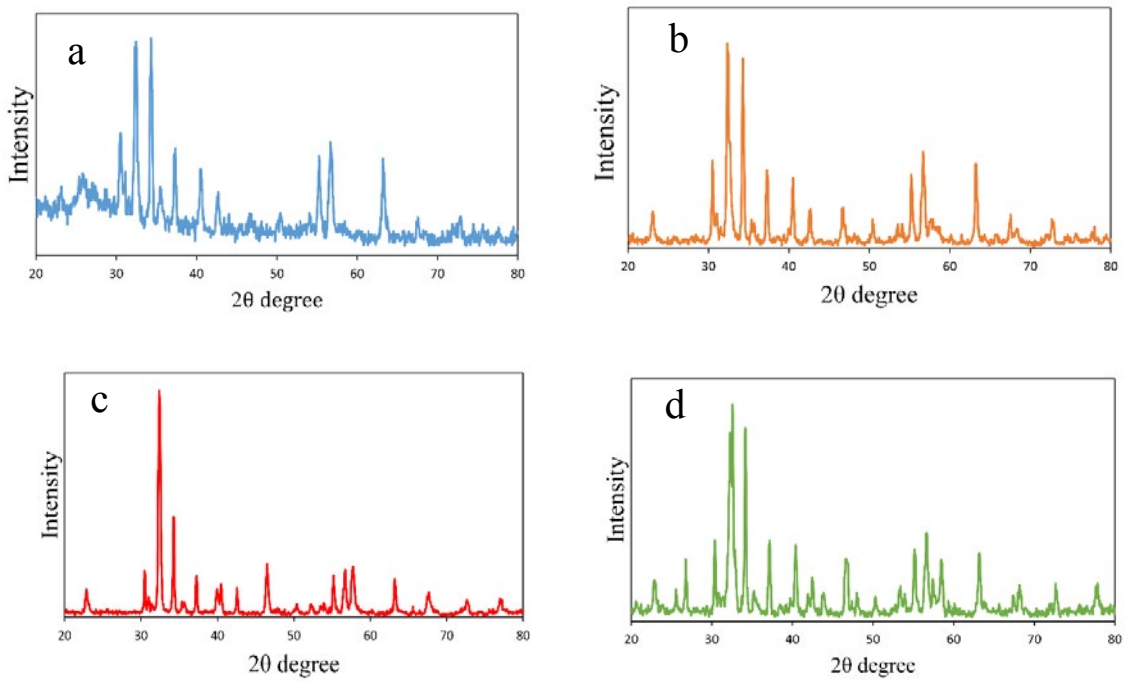

Fig. 2. XRD $BaLa_xGd_xFe_{12-2x}O_{19}$ a) x=0.2, b) 0.4, c) 0.6 and d) 0.8

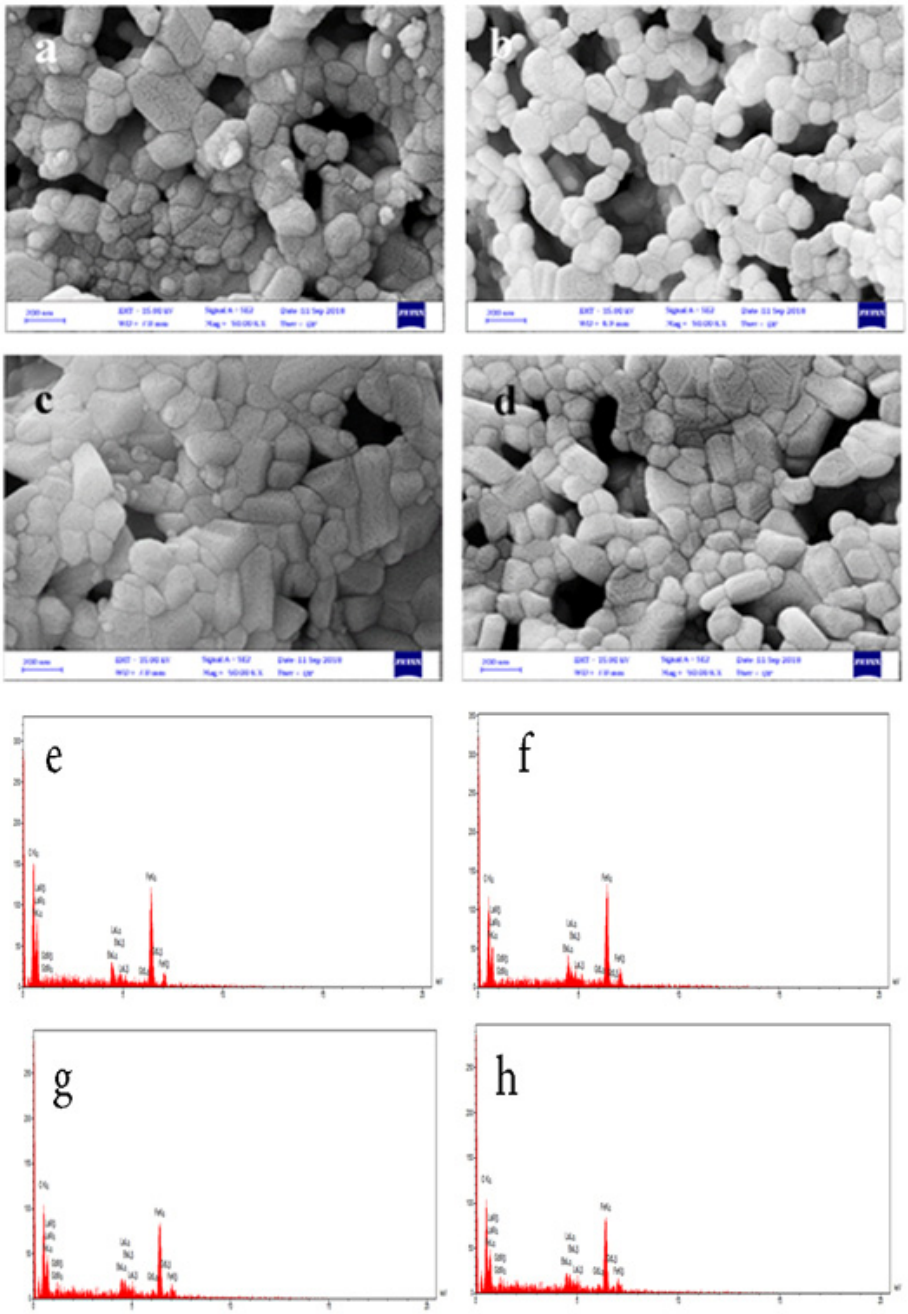

Fig. 3. FESEM image of $BaLa_xGd_xFe_{12-2x}O_{19}$ a) x=0.2, b) 0.4, c) 0.6 and d) 0.8 and EDX analysis of $BaLa_xGd_xFe_{12-2x}O_{19}$ e) x=0.2, f) 0.4, g) 0.6 and h) 0.8

the crystallite size were increased from 68.90 to 119.25 nm (Table 1). The lattice parameters of the samples were revealed in Table 1.

FESEM images

FESEM images of $BaLa_xGd_xFe_{12-2x}O_{19}$ (x=0.2, 0.4, 0.6 and 0.8) were represented in Fig. 3. The hexagonal shapes of barium hexaferrite were observed at the pictures. Agglomeration of samples were due to the magnetic properties of barium hexaferrite. The porosity of samples were observed in all pictures. The average particle size of $BaLa_xGd_xFe_{12-2x}O_{19}$ (x=0.2, 0.4, 0.6 and 0.8) for different substitution values, were about 84, 117, 144 and 165nm. By enhancing the dopant values, the average particle size were increased from 52

to 165 nm. According to the average particle sizes of barium hexaferrites which were smaller than the critical values (650 nm), the samples have belonged to the single domain wall material (21).

The EDX analysis of all the samples were prepared. Due to the EDX analysis, the presence of all elements was indicated.

VSM analysis

VSM magnetic analysis of samples were represented in Fig. 4. According to the coercivity values (Table 2) of all samples (about 5000 Oe), $BaLa_xGd_xFe_{12-2x}O_{19}$ (x=0.2, 0.4, 0.6 and 0.8) were classified into the hard magnetic materials. Iron in hexaferrite structures were occupied five different positions (three octahedral sites (*12k*, *2a*, and $4f_2$), one tetrahedral site ($4f_1$) and one trigonal bipyramidal site (*2b*)). By adding La^{3+} as a dopant, the saturation magnetization were decreased (63.81 to 51.78 emu/g). La^{3+}. Non-magnetic La^{3+} were occupied octahedral spin up positions which decreased the whole net magnetic moment (63.81 to 36.56 emu/g). On the other hand, replacing La^{3+} on the crystal structure of hexaferrite can cause distortion especially cationic vacancies which enhance spin casting effects and consequently reduce the saturation magnetization. When Fe^{3+} substituted by Gd^{3+}, the superexchange interactions of Fe^{3+}-O-Fe^{3+} reduced. High differences of ionic radii of La^{3+} (1.22Å), Gd^{3+} (1.07Å) and Fe^{3+} (0.63Å) increase the distance between the magnetic ions and reduce the interactions which cause the reduction of M_s (22-26). According to the $H_c = 2k / \mu_0 M_s$ equation (in which H_c is coercivity, μ_0 is the permeability of free space, k is magnetocrystalline anisotropy constant and M_S is saturation magnetization), by decreasing M_s, the coercivity increased from 5000 to 5500 Oe. M_r/M_s ratio or squareness ratios of samples are in the range of 0.4-0.6 which could select each sample

Table 2. Magnetic data of $BaLa_xGd_xFe_{12-2x}O_{19}$ (x=0.2, 0.4, 0.6 and 0.8)

samples	M_s(emu/g)	M_r	M_r/M_s	H_c(Oe)
X=0	64	29.31	0.5	5010
X=0.2	63.81	32.77	0.5	5000
X=0.4	51.78	31.41	0.6	5000
X=0.6	42.33	20.99	0.4	5500
X=0.8	36.56	25.56	0.6	5500

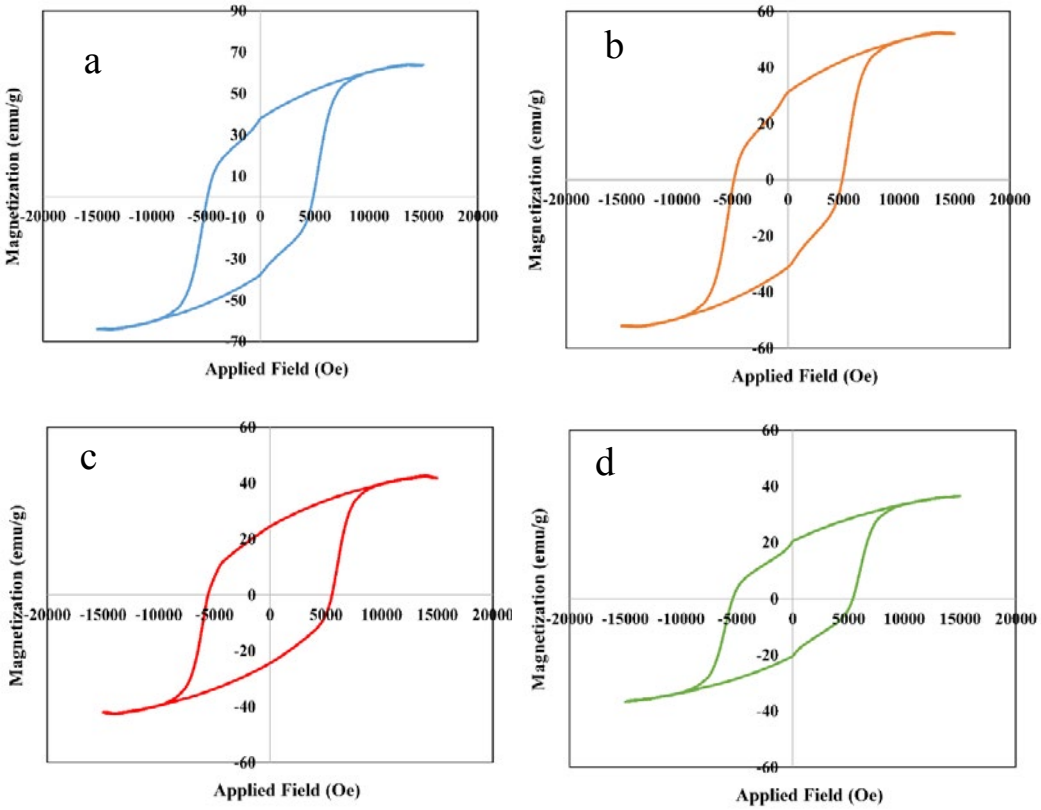

Fig. 4. Magnetic hysteresis loops of $BaLa_xGd_xFe_{12-2x}O_{19}$ a) x=0.2, b) 0.4, c) 0.6 and d) 0.8

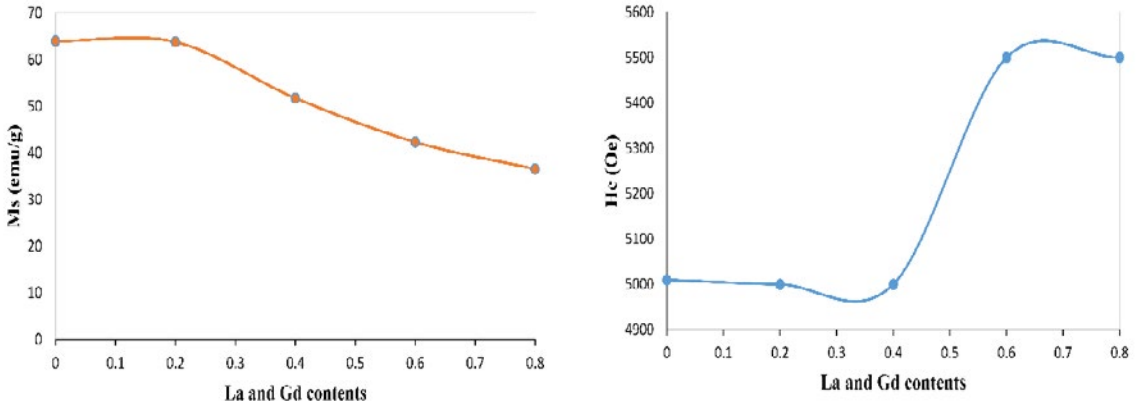

Fig. 5. coercivity and saturation magnetization of $BaLa_xGd_xFe_{12-2x}O_{19}$ (x=0.2, 0.4, 0.6 and 0.8) versus dopants contents

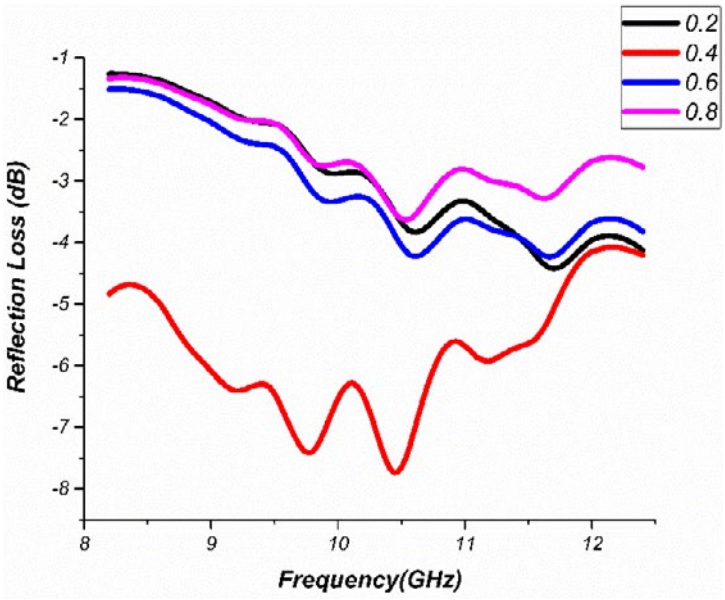

Fig. 6. Reflection loss of $BaLa_xGd_xFe_{12-2x}O_{19}$ (x=0.2, 0.40.6 , 0.8)

in various industrial applications. Variations of the saturation magnetization and the coercivity of $BaLa_xGd_xFe_{12-2x}O_{19}$ (x=0.2, 0.4, 0.6 and 0.8) versus dopants content were represented in Fig. 5. By increasing the dopants content, M_s *(emu/g)* were decreased while H_c *(Oe)* were increased.

VNA Analysis

Microwave absorption properties of products was studied by reflection loss, consequently, the reflection loss can be calculated by following equation (3) and (4):

$$R\left(db\right)=20log\left|\frac{Z_{in}-1}{Z_{in}+1}\right| \quad (3)$$

$$Z_{in}=\sqrt{\mu_r/\varepsilon_r}\,tanhj\left(\frac{2\pi}{c}\right)\sqrt{\mu_r\varepsilon_r}fd \quad (4)$$

In this equations, Z_{in} is the input impedance, μ_r is the permeability, ε_r is the permittivity, *f* is the microwave, *c* is the light velocity and *d* is the thickness of the absorbing layer.

The reflection loss versus frequency (in the X-band: 8-12 GHz) curves was presented in Fig. 6. The reflection loss value for x=0 was not observable. For x=0.2 the reflection loss value was reached to the -3.6 db at 10.4 GHz frequency. For x=0.6 the reflection loss value was increased to the -4 db at 10.6 GHz frequency. Then, at x= 0.8 the reflection loss value was enhanced to -3.5 db at

10.5 GHz frequency. The highest value of reflection loss was -7.8 db at 10.4 GHz frequency for x=0.4. By increasing rare earth dopants, the microwave absorption properties improved. In comparison to the pure barium hexaferrites which represented maximum reflection loss of -2 db without any strong peak, the doped products indicate better and sharper microwave absorption properties.

CONCLUSION

$BaLa_xGd_xFe_{12-2x}O_{19}$ (x=0.2, 0.4, 0.6 and 0.8) were synthesized successfully via sol-gel auto-combustion method. FTIR spectrums were represented two bands at 400 and 500 cm^{-1} which were related to the vibrating modes of tetrahedral and octahedral vibrations. XRD patterns were revealed the formation of pure barium hexaferrite without any impurities. The crystallite data were revealed that due to the bigger radius of La^{3+} and Gd^{3+} rather than Fe^{3+}, lattice parameters such as *a, c* and crystallite size were increased. Hexagonal shapes of barium hexaferrite were seen in all samples. The synthesized samples have belonged to the single domain wall materials. All samples were divided into the hard magnetic materials. By substituting La^{3+} and Gd^{3+} instead of Fe^{3+}, the saturation magnetization were decreased due to the non-magnetic properties of rare earth. The coercivity of samples were increased by substitution of dopants because of the reverse relation of coercivity and saturation magnetization. The highest value of reflection loss was -7.8 db at 10.4 GHz frequency in 3mm thickness for x=0.4 sample.

CONFLICT OF INTEREST

The authors declare that there are no conflicts of interest regarding the publication of this manuscript.

REFERENCES

1. Pullar RC. Hexagonal ferrites: A review of the synthesis, properties and applications of hexaferrite ceramics. Progress in Materials Science. 2012;57(7):1191-334.
2. soloveva. Structural and Magnetic Properties of $BaFe_{12-2x}$ Modified M-Type Hexaferrites.J Inorganic Materials, 2012;48:223-231.
3. Zhang Z. Electromagnetic and microwave absorption properties of Fe–$Sr_{0.8}La_{0.2}Fe_{11.8}Co_{0.2}O_{19}$ shell-core composites. J MagnetismandMagneticMaterials, 2012;324:122-129.
4. Iqbal MJ. Physical, electrical and dielectric properties of Ca-substituted strontium hexaferrite ($SrFe_{12}O_{19}$) nanoparticles synthesized by co-precipitation method. J Magnetism and Magnetic Materials, 2017;322:103-111.
5. Mehdipour M. Comparison of microwave absorption properties of $SrFe_{12}O_{19}$, $SrFe_{12}O_{19}/NiFe_2O_4$, and $NiFe_2O_4$ particles. J Appl Phys, 2013;114:815-823.
6. Ozah S, Bhattacharyya NS. Development of BaAlxFe12−xO19-NPR nanocomposite as an efficient absorbing material in the X-band. Journal of Magnetism and Magnetic Materials. 2015;374:516-24.
7. Sharma R, Singhal S. Structural, magnetic and electrical properties of zinc doped nickel ferrite and their application in photo catalytic degradation of methylene blue. Physica B: Condensed Matter. 2013;414:83-90.
8. Stergiou CA, Litsardakis G. Electromagnetic properties of Ni and La doped strontium hexaferrites in the microwave region. Journal of Alloys and Compounds. 2011;509(23):6609-15.
9. Wang JF, Ponton CB, Harris IR. A study of Pr-substituted strontium hexaferrite by hydrothermal synthesis. Journal of Alloys and Compounds. 2005;403(1-2):104-9.
10. Luo J. Structural and magnetic properties of Nd-doped strontium ferrite nanoparticles. Materials Letters. 2012;80:162-4.
11. wang l. XAFS and XPS studies on site occupation of Sm^{3+} ions in Sm doped M-type $BaFe_{12}O_{19}$. J Magnetism and Magnetic Materials, 2015;377:84-92.
12. Ataie A, Harris IR, Ponton CB. Magnetic properties of hydrothermally synthesized strontium hexaferrite as a function of synthesis conditions. Journal of Materials Science. 1995;30(6):1429-33.
13. Alam RS, Moradi M, Rostami M, Nikmanesh H, Moayedi R, Bai Y. Structural, magnetic and microwave absorption properties of doped Ba-hexaferrite nanoparticles synthesized by co-precipitation method. Journal of Magnetism and Magnetic Materials. 2015;381:1-9.
14. Haijun Z, Zhichao L, Chengliang M, Xi Y, Liangying Z, Mingzhong W. Complex permittivity, permeability, and microwave absorption of Zn- and Ti-substituted barium ferrite by citrate sol–gel process. Materials Science and Engineering: B. 2002;96(3):289-95.
15. Mosleh Z, Kameli P, Poorbaferani A, Ranjbar M, Salamati H. Structural, magnetic and microwave absorption properties of Ce-doped barium hexaferrite. Journal of Magnetism and Magnetic Materials. 2016;397:101-7.
16. Shooshtary Veisi S, Yousefi M, Amini MM, Shakeri AR, Bagherzadeh M. Magnetic and microwave absorption properties of Cu/Zr doped M-type Ba/Sr hexaferrites prepared via sol-gel auto-combustion method. Journal of Alloys and Compounds. 2019;773:1187-94.
17. Ounnunkad S. Improving magnetic properties of barium hexaferrites by La or Pr substitution. Solid State Communications. 2006;138(9):472-5.
18. Shlyk L. Single crystal growth, structural characteristics and magnetic properties of chromium substituted M-type ferrites. H Solid State Sciences, 2015;50:23-31.
19. Rai B.K, Mishra S.R. Synthesis and characterization of high coercivity rare-earth ion doped
$Sr_{0.9}RE_{0.1}Fe_{10}Al_2O_{19}$ (RE: Y, La, Ce, Pr, Nd, Sm, and Gd). J Alloys and Compounds, 2013; 550: 198-203.
20. Chen J. Electromagnetic and microwave absorption properties of $BaMg_xCo_{1-x}TiFe_{10}O_{19}$. J Alloys and Compounds,2016; 679: 335-340.
21. Ghezelbash S, Yousefi M. Structural and Magnetic Properties of Sn^{4+} Doped Strontium Hexaferrites Prepared via Sol–Gel Auto-Combustion Method. J IEEE Transaction

on magnetics, 2018;54: 1-6.
22. Yanbing H, Sha J, Lina S, Quan T, Qin L, Hongxiao J. Tailored magnetic properties of Sm(Zn) substituted nanocrystalline barium hexaferrites. J Alloys and Compounds, 2009;486(1-2):348-51.
23. Thakur A. Structural and magnetic properties of La^{3+} substituted strontium hexaferrite nanoparticles prepared by citrate precursor method. j Magnetism and Magnetic Materials, 2013; 326: 35-40.
24. Ashiq MN, Shakoor S, Najam-ul-Haq M, Warsi MF, Ali I, Shakir I. Structural, electrical, dielectric and magnetic properties of Gd-Sn substituted Sr-hexaferrite synthesized by sol–gel combustion method. Journal of Magnetism and Magnetic Materials. 2015;374:173-8.
25. stergiou A. Dielectric and magnetic properties of new rare-earth substituted Ba-hexaferrites in the 2–18GHz frequency range. J Magnetism and Magnetic Materials,2010; 322(9-12):1532-1535.
26. Anterpreet S, Bindra S, Kulwant S, Pandeyd O.P. Electrical and magnetic properties of rare earth substituted strontium hexaferrites. J Ceramic Processing Research, 2010; 11(2): 241-249.